Electronical Supplementary Information: Spectroscopic analysis of vibrational coupling in multi-molecular excited states

Sebastian Hammer*[1,4], Theresa Linderl[2], Kristofer Tvingstedt[1], Wolfgang Brütting[2], and Jens Pflaum†[1,3]

[1]Experimental Physics VI, Julius Maximilian University Würzburg, 97074 Würzburg, Germany.
[2]Institute of Physics, University of Augsburg, 86135 Augsburg, Germany.
[3]Bavarian Center for Applied Energy Research, 97074 Würzburg, Germany.
[4]Present address: Center for the Physics of Materials, Department of Physics and Department of Chemistry, McGill University, Montreal, QC H3A 2K6, Canada.

*mail to: sebastian.hammer@mail.mcgill.ca
†mail to: jens.pflaum@physik.uni-wuerzburg.de

Supplementary note 1: Semi-classical model of excimer emission

As described in the main manuscript, the probability of the X-dimer geometry to adopt the displacement q^* is given by the probability density $|\Psi(q^*)|^2 \, dq$ which is directly related to the emission spectrum $\overline{I}(E) dE$ for a photon energy E by

$$\overline{I}\left(E\left(q^*\right)\right) dE = \left|\Psi\left(q^*\right)\right|^2 dq. \tag{S1}$$

Furthermore, the spatial coordinate q can be expressed as a function of the photon energy $q(E)$, and with an appropriate Jacobian for the coordinate transformation the emission spectrum for a transition from an excited state $|X, n\rangle$ to the electronic ground state reads

$$\overline{I}_n\left(E\right) dE = \left|\Psi_n\left(q\left(E\right)\right)\right|^2 \frac{dq}{dE} dE \tag{S2}$$

with the wave function Ψ_n as the wave function of the vibrational state $|n\rangle$. This expands the semi-classical temperature dependent emission spectrum as given by equation (9) in the manuscript by

$$\begin{aligned}
\overline{I}\left(E, T\right) dE &= \sum_n P\left(n, T\right) \overline{I}_n\left(E\right) dE \\
&= \sum_n P\left(n, T\right) \left|\Psi_n\left(q\left(E\right)\right)\right|^2 \frac{dq}{dE} dE.
\end{aligned} \tag{S3}$$

To establish an analytical relation between the spatial coordinate and the photon energy, we use equations (3), (5) and (6) from the main text to calculate the photon energy and define the respective spatial coordinate for a vibrational X-dimer state $|n\rangle$ defined by equation (4) in the main text to

$$\tilde{q}_n\left(E\right) = \sqrt{\frac{E_{\mathrm{X,n}} - E}{R_0}} - q_e \tag{S4}$$

yielding

$$\frac{d\tilde{q}_n}{dE} = \frac{1}{2\sqrt{R_0\left(E_{\mathrm{X,n}} - E\right)}} \tag{S5}$$

as the Jacobian. Using the wave functions of the quantum mechanical harmonic oscillator, see e.g.[1],

$$\psi_n\left(\tilde{q}_n\right) = \left(\frac{\alpha}{\pi}\right)^{\frac{1}{4}} \frac{1}{\sqrt{2^n n!}} H_n\left(\sqrt{\alpha}\tilde{q}_n\right) \exp\left(-\frac{1}{2}\alpha\tilde{q}_n^2\right) \tag{S6}$$

with the respective hermite polynome $H_n(x)$ and an oscillator parameter $\alpha = \mu E_{\mathrm{X,vib}}/\hbar^2$ the emission spetrum $\overline{I}_n\left(E\right) dE$ defined in equation (S2) can be expressed analytically using equations (S4)-(S6).

Evaluating (S2) for the emission $|X, n\rangle \rightarrow |G\rangle$ from the first six vibrational levels $n \in \{0, 1, 2, 3, 4, 5\}$ yields

$$\overline{I}_0(E)\mathrm{d}E = \frac{1}{2}\sqrt{\frac{\alpha}{R_0\pi\left(E_{\mathrm{X},0} - E\right)}}\,\exp\left(-\alpha\tilde{q}_0^2\right)\mathrm{d}E \tag{S7}$$

$$\overline{I}_1(E)\mathrm{d}E = \sqrt{\frac{\alpha}{R_0\pi\left(E_{\mathrm{X},1} - E\right)}}\,\alpha\tilde{q}_1^2\,\exp\left(-\alpha\tilde{q}_1^2\right)\mathrm{d}E \tag{S8}$$

$$\overline{I}_2(E)\mathrm{d}E = \frac{1}{4}\sqrt{\frac{\alpha}{R_0\pi\left(E_{\mathrm{X},2} - E\right)}}\left(2\alpha\tilde{q}_2^2 - 1\right)^2\exp\left(-\alpha\tilde{q}_2^2\right)\mathrm{d}E \tag{S9}$$

$$\overline{I}_3(E)\mathrm{d}E = \frac{1}{6}\sqrt{\frac{\alpha}{R_0\pi\left(E_{\mathrm{X},3} - E\right)}}\left(2\alpha\tilde{q}_3^2 - 3\right)^2\alpha\tilde{q}_3^2\,\exp\left(-\alpha\tilde{q}_3^2\right)\mathrm{d}E \tag{S10}$$

$$\overline{I}_4(E)\mathrm{d}E = \frac{1}{48}\sqrt{\frac{\alpha}{R_0\pi\left(E_{\mathrm{X},4} - E\right)}}\left(4\alpha^2\tilde{q}_4^4 - 12\alpha\tilde{q}_4^2 + 3\right)^2\exp\left(-\alpha\tilde{q}_4^2\right)\mathrm{d}E \tag{S11}$$

$$\overline{I}_5(E)\mathrm{d}E = \frac{1}{120}\sqrt{\frac{\alpha}{R_0\pi\left(E_{\mathrm{X},5} - E\right)}}\left(\left(2\alpha\tilde{q}_5^2 - 5\right)^2 - 10\right)^2\alpha\tilde{q}_5^2\,\exp\left(-\alpha\tilde{q}_5^2\right)\mathrm{d}E \tag{S12}$$

Supplementary note 2: Numerical evalution of the quantum-mechanical overlap intergral

The $\propto \exp\left(-q^2\right)$ dependency of the oscillator wave functions (S6) enables a straightforward numerical integration applying fixed suitable boundaries as the wave function only slightly extends beyond the turning points of the classical oscillator at any given energy. Hence, equation (10) of the main manuscript simplifies to

$$\langle m \,|\, n \rangle = \int_{-\Delta q}^{\Delta q} \Phi_m^*\left(q\right) \Psi_n\left(q - q_e\right) \mathrm{d}q. \tag{S13}$$

The integration interval $[-\Delta q, \Delta q]$ has to be chosen as such, that it almost fully includes the ground state wave function $\Phi_m\left(q\right)$ located around $q = 0$ and the excited state wave function $\Psi_n\left(q - q_e\right)$ at $q = q_e$. Suitable integration boundaries can be estimated using the classical turning points of a harmonic oscillator with oscillator constant R as

$$q = \sqrt{\frac{2\left(n + \frac{1}{2}\right) E_{\mathrm{vib}}}{R}} \tag{S14}$$

where E_{vib} represents the vibrational energy quantum. For an exemplary reduced mass of $\mu = 350\,\mathrm{u}$ and a vibrational energy quantum $E_{\mathrm{vib}} = 20\,\mathrm{meV}$ equation(S14) yields $q(n = 5) = 0.1\,\text{Å}$, $q(n = 10) = 0.22\,\text{Å}$ and $q(n = 25) = 0.34\,\text{Å}$. For a common spatial displacement of $q_e \approx 0.2\,\text{Å}$ this means that for integration boundaries of $\Delta q = \pm 0.5\,\text{Å}$ even excited state wave functions as high as $n = 10$ are almost completely included while the ground state wave functions are included even up to $n = 25$. The numerical integration is performed using the "simpson" integration function within the SciPy python package [2].

Of course, equation (10) in the main manuscript has to be evaluated for all transitions $|X, n\rangle \rightarrow |G, m\rangle$ contributing to the emission spectrum at temperature T and hence the maximum evaluated vibrational levels of the ground and X-dimer state, $M := \{0, 1, \ldots, m_{\mathrm{max}}\}$ and $N = \{0, 1, \ldots, n_{\mathrm{max}}\}$, respectively, have to be chosen accordingly. This results in a total of $|N \times M|$ individual transitions which need to be calculated. To minimize evaluation time during fit procedures, n_{max} should be chosen according to the excepted vibrational energy quantum of the X-dimer state and the highest temperature. For example, as indicated in note 62 in the main manuscript, for a vibrational energy quantum of $25\,\mathrm{meV}$ and a temperature of $400\,\mathrm{K}$ the population probability of the 5th vibrationally excited state is $1.4\,\%$.

Supplementary note 3: Computational details for simulated emission spectra in figure 3

The emission spectra presented in figure 3 in the main manuscript have been generated by assuming a reduced mass of $\mu = 288.958\,\mathrm{u}$ (corresponding to the reduced mass of a zinc-phthalocyanine dimer). The constant parameters where chosen as $E_{\mathrm{vib,G}} = 25\,\mathrm{meV}$ for the ground state vibrational energy, $D_e = 2\,\mathrm{eV}$ as the energetic offset, $q_e = 0.1\,\mathrm{\AA}$ as the spatial offset and $\sigma = 20\,\mathrm{meV}$ as the line width parameter of the gaussian line shape function. For the steep and shallow X-dimer state we set $E_{\mathrm{vib,X}} = 30\,\mathrm{meV}$ and $E_{\mathrm{vib,X}} = 20\,\mathrm{meV}$, respectively. Emission spectra where simulated in $5\,\mathrm{K}$ steps from $5\,\mathrm{K}$ to $400\,\mathrm{K}$ and in $25\,\mathrm{K}$ steps between $400\,\mathrm{K}$ and $1000\,\mathrm{K}$ considering 100 vibrational levels for the ground state oscillator and 20 vibrational levels for the X-dimer state. The Boltzmann population has been numercially evaluated assuming $z = 100$ vibrational states of the X-dimer. The numerical integration has been performed within $\Delta Q = \pm 3\,\mathrm{\AA}$.

Figure S1 shows the peak maximum (dots) as well as the asymmetric half-width-half-maximum (HWHM) towards the low and high energy side of the spectrum (bars) for selected temperatures between $5\,\mathrm{K}$ and $400\,\mathrm{K}$ illustrating the broadening of the spectra as well as the maximum peak shift with temperature.
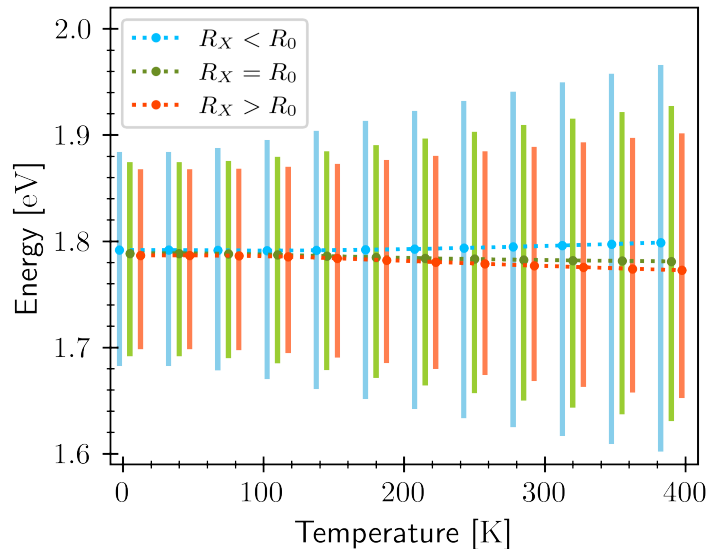

Figure S1: Maximum peak position (dots) and the HWHM to the low and high energy side (bars) with temperature for all three cases. Dotted lines as guide-to-the-eye for the peak shift.

The evolution of the peak shift with temperature is also shown in figures S2 a) and b) for different temperature ranges indicating the different trends towards higher and lower emission energies for all three cases of potential strengths. To provide deeper insight into the temperature dependence of the asymmetry between high and low energy flank of the emission spectra figures S2 c) and d) depict the ratio between the HWHM of low and high energy flank of the simulated emission spectra. The ratio is calculated as

$$R = \frac{HWHM_{\mathrm{low\ energy}}}{HWHM_{\mathrm{high\ energy}}}. \tag{S15}$$

Hence, a value of $R = 1$ indicates a symmetric emission profile while values of $R < 1$ and $R > 1$ indicate an asymmetry towards the low and high energy flank, respectively. For

the case of the weaker excited state potential we see $R < 1$ over the whole temperature range showing the asymmetry towards the low energy side, while for the stronger excited state potential the assymetry changes from the low to the high energy flank with rising temperature. For the case of the equal ground and excited state potential R converges towards 1 with rising temperature, which means the spectrum strives towards a symmetric emission profile.
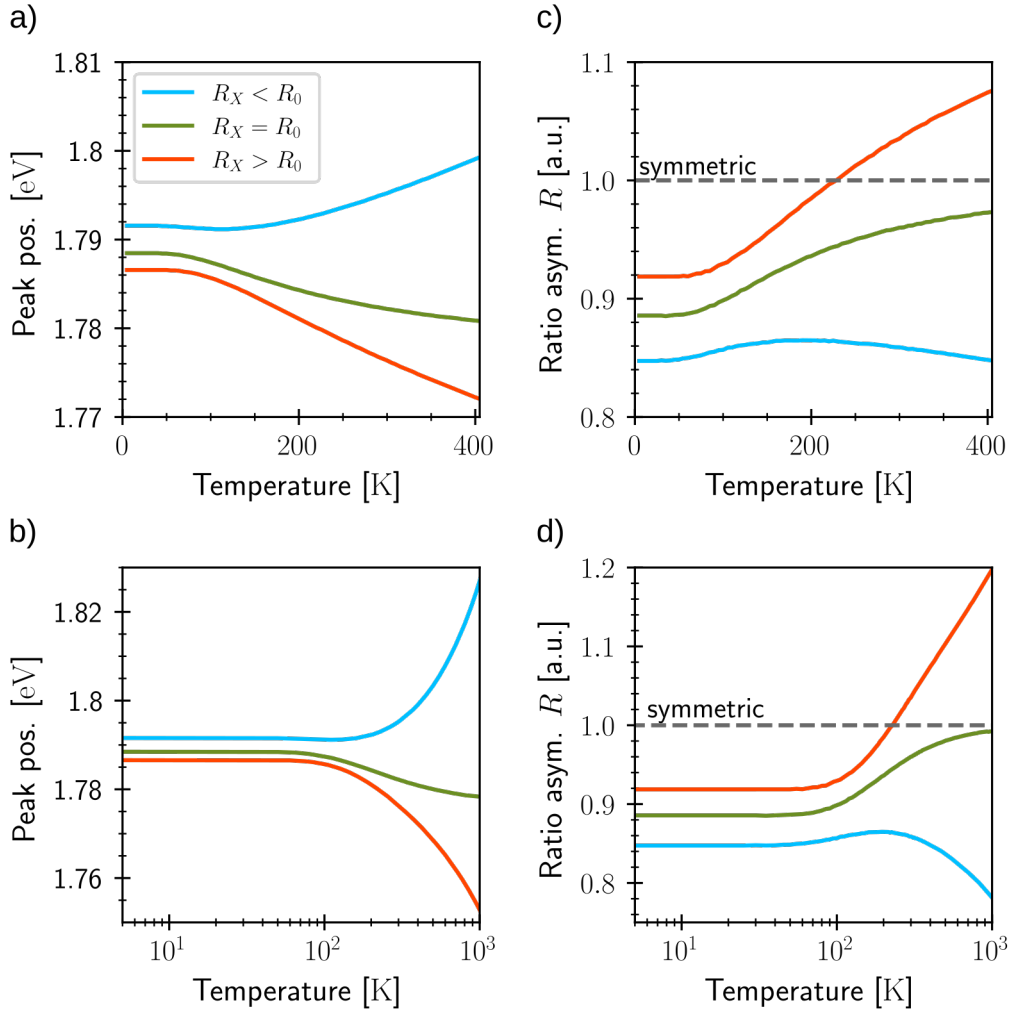

Figure S2: Maximum peak positions (a, b) as well as ratio of the low and high energy side HWHM (c,d) as a function of temperature. A ratio of one indicates a symmetric emission profile, while values smaller/larger than one indicate an asymmetry towards the low/high energy side.

Supplementary note 4: Estimation of the zero point energy from the FWHM temperature of the α-ZnPc emission spectra

The FWHM of the temperature dependent α-ZnPc emission spectra has been extracted by the abscissa difference between the half-intensity point of the low and high energy flank of a smoothed spectral curve. The errors are estimated from the noise of the spectral curve. The data was fitted using equation (14) from the main manuscript yielding the fit parameters $P_0 = (147.9 \pm 1.4)\,\text{meV}$ and $T_0 = \frac{E_{0,\text{X}}}{k_b} = (171.4 \pm 5.2)\,\text{K}$.
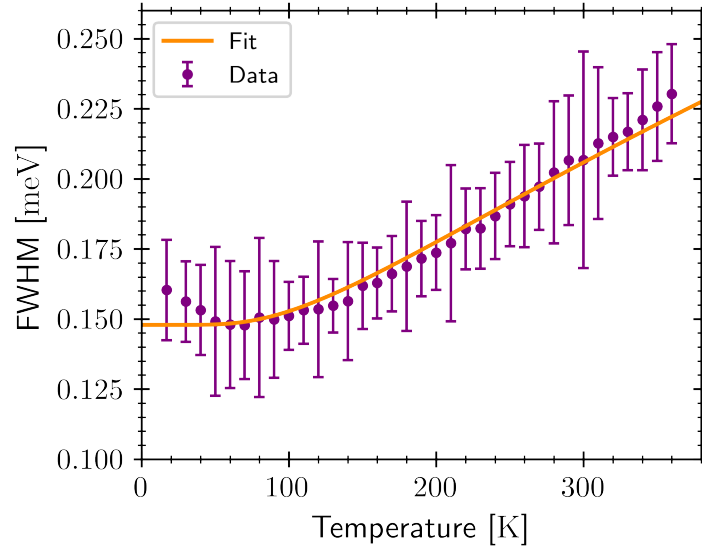
Figure S3: ZnPc FWHM with temperature together with fit curve from equation (14).

Supplementary note 5: ZnPc emission: X-dimer model

Extracted fitting parameters from the quantum mechanical and semi-classical X-dimer model are shown in figures S4 and S5, respectively. Figures S6 and S7 show the full data set of the temperature dependent photoluminescence data including the fit curves for the quantum mechanical and semi-classical approach, respectively.
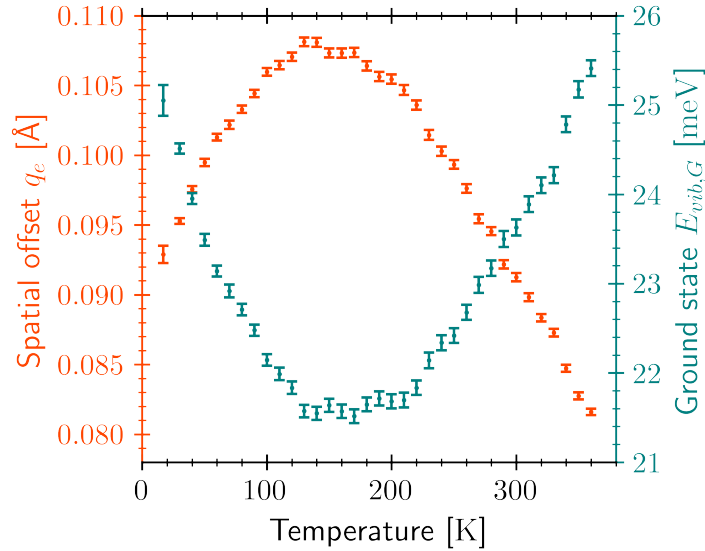

Figure S4: Temperature dependence of spatial offset q_e (orange, left y-axis) and vibratioanl energy of the ground state $E_{\mathrm{vib,G}}$ (teal, left y-axis) extracted from the quantum mechanical X-dimer fit to the ZnPc luminescence data.
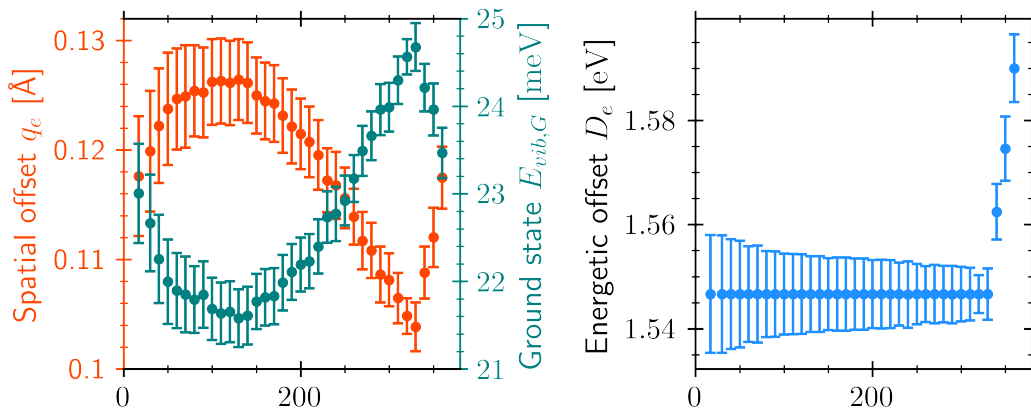

Figure S5: Temperature dependence of spatial offset q_e (orange, left y-axis) and vibrational energy of the ground state $E_{\mathrm{vib,G}}$ (teal, left y-axis) (a) as well as energetic offset D_e (b) extracted from the semi-classical X-dimer fit to the ZnPc luminescence data.
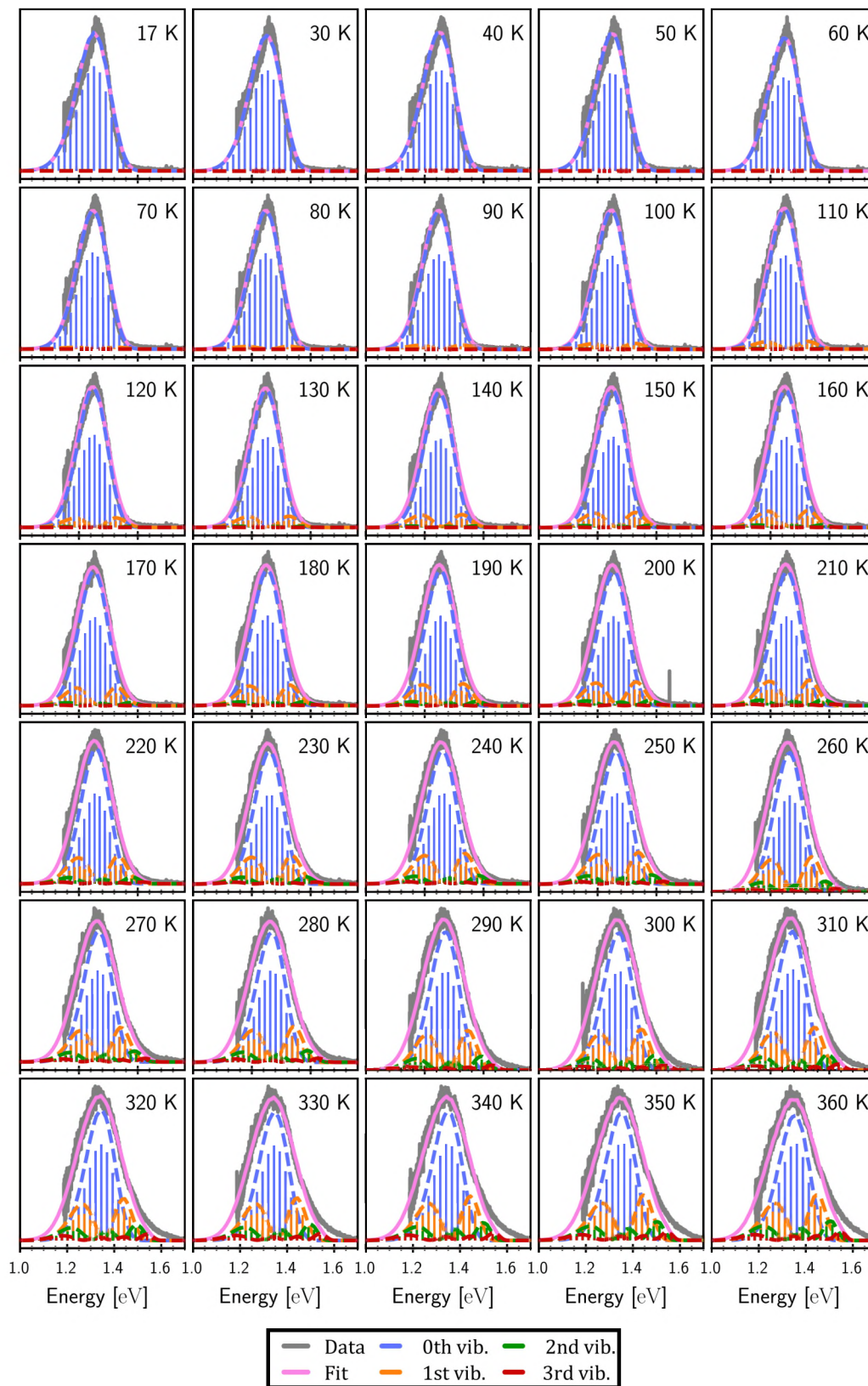
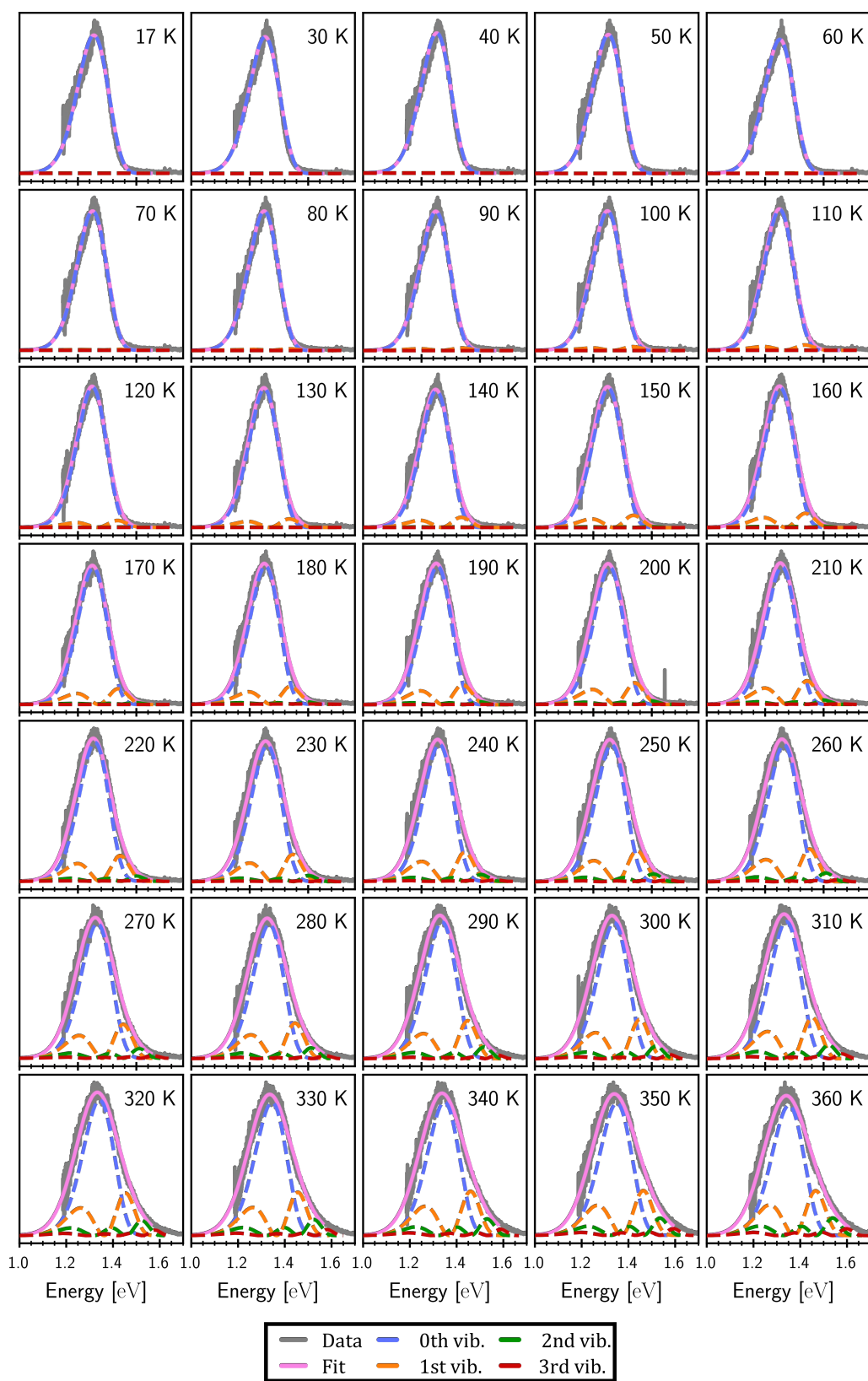Figure S6: ZnPc emission spectra fitted with quantum mechanical X-dimer model.

9

Figure S7: ZnPc emission spectra fitted with semi-classical X-dimer model.

References

[1] W. W. Parson, *Modern optical spectroscopy*, Springer, Berlin Heidelberg, 2007, vol. 2.

[2] P. Virtanen, , R. Gommers, T. E. Oliphant, M. Haberland, T. Reddy, D. Cournapeau, E. Burovski, P. Peterson, W. Weckesser, J. Bright, S. J. van der Walt, M. Brett, J. Wilson, K. J. Millman, N. Mayorov, A. R. J. Nelson, E. Jones, R. Kern, E. Larson, C. J. Carey, İ. Polat, Y. Feng, E. W. Moore, J. VanderPlas, D. Laxalde, J. Perktold, R. Cimrman, I. Henriksen, E. A. Quintero, C. R. Harris, A. M. Archibald, A. H. Ribeiro, F. Pedregosa and P. van Mulbregt, *Nature Methods*, 2020, **17**, 261–272.